Polymer(Korea), Vol. 42, No. 6, pp. 910-918 (2018)
https://doi.org/10.7317/pk.2018.42.6.910
ISSN 0379-153X(Print)
ISSN 2234-8077(Online)

토션엘리먼트가 있는 단축압출기의 균질화 구간에서 고분자 용융액의 혼합 성능 향상에 대한 수치모사

Ranran Jian, Weimin Yang†, Lisheng Cheng, and Pengcheng Xie
College of Mechanical and Electrical Engineering, Beijing University of Chemical Technology
(2018년 2월 28일 접수, 2018년 4월 16일 수정, 2018년 5월 23일 채택)

Numerical Simulation on the Enhanced Mixing of Polymer Melt by Single Screw with Torsion Elements in the Homogenizing Section

Ranran Jian, Weimin Yang†, Lisheng Cheng, and Pengcheng Xie
College of Mechanical and Electrical Engineering, Beijing University of Chemical Technology, Beijing100029, China
(Received February 28, 2018; Revised April 16, 2018; Accepted May 23, 2018)

Abstract: As one of key factors that determine the quality of products, the homogenization of polymer melt is closely dependent on the mixing of polymers. The mixing of polymer melt in the homogenizing section by a single screw with torsion elements was analyzed with the computational fluid dynamics (CFD) simulation. The simulation results reveal that screws with such torsion elements arranged in a decentralized form have smaller segregation scale, distribution index and higher mixing efficiency, compared with the conventional screw. The decentralized arrangement is more effective for mixing than the centralized distribution. The rotational flow induced by the torsion elements can significantly enhance the mass transfer process and improve mixing and plasticizing. Compared with those in conventional screw, the distributions of temperature and viscosity are more uniform at the outlet of torsion screws, which also made the torsion element generally more effective and efficient for mixing and plasticizing.

Keywords: torsion element, distributive mixing, dispersive mixing, mixing efficiency, plasticizing quality.

Introduction

In both extrusion and injection molding, the homogeneity of polymer melt is determined for the quality of product,[1,2] thus various of screw geometries[3-5] and mixing elements[6,7] have been designed to improve the homogeneity of polymer melt. Mixing contributes to mass transfer, distributes physical property of ingredients more uniform including temperature, viscosity, etc. throughout three ways: disturbing flow, shear flow and elongation flow. The plasticizing effect can therefore be evaluated by looking at the mixing ability of the screw plasticizing unit to distribute ingredients and mass transfer enhancement.[8]

There are three main approaches to enhance mixing of polymer melts in the screw plasticizing unit. The first is by making use of disturbing flow or rotational flow. Among them the pin screw is one important mixing unit, and has drawn many explorations. Hwang *et al.*[9] studied the influence of pin configurations on the screw's mixing properties with dynamical systems theory, and results showed that the existence of the pin can generate a perturbation for large-scaled orbits of fluid particle, and generate elliptic rotations for small-scaled orbits. Yao *et al.*[10] investigated the effect of the pin distance on the mixing of polymer melt in a pin screw extruder, and evaluated the mixing performance quantitatively from the aspect of integral mixing efficiency and residence time distribution (RTD). Li *et al.*[11] proposed nine arrays of pin mixing sections through orthogonal designing and systematically discussed the effects of their height and arrangements on the efficiency of mixing.

The second way to promote mixing of polymer melt is through the enhancement of shear, such as the application of Maddock and spiral shearing sub-sections. Zitzenbacher *et al.*[12] presented a new calculation model to optimize the structure of fluted mixing sections, such as axial and spiral Maddock-ele-

†To whom correspondence should be addressed.
yangwm@mail.buct.edu.cn, ORCID 0000-0001-5471-3151

ments and Z-elements. Kubik *et al.*[13] studied the mixing abilities of stratablend II mixer and two similarly designed Maddock mixers, and found that better mixing could be obtained with higher shear stress on average. Hu *et al.*[14] designed a powerful shear mixer, and the results showed that the particles of T-ZnOw were dispersed more uniformly in the epoxy matrix mixed by the powerful shear mixer compared with those by traditional methods. Feng *et al.*[15] introduced a vibration force field into the extrusion process by the axial vibration of screw, which resulted in the increasement of total shear strain of melt and was favorable for melt mixing.

The third way to improve mixing is by incorporating elongational flows. Bouquey *et al.*[16] built a laboratory-scale mixing device and indicated that the elongational flow mixer had more uniform size distribution of dispersed particles than a rotary mixer with equivalent input of specific energy. Qu *et al.*[17-19] proposed a novel vane extruder based on elongational rheology and volume transportation. Their results showed that the vane extruder had good mixing ability and plasticizing capacity. Wen *et al.*[20,21] also studied the mixing abilities of vane extruder by numerical analysis found that there existed strong stretching of melt in the vane extruder. Yin *et al.*[22] successfully prepared polypropylene nanocomposites with halloysite nanotubes (HNTs) through a vane extruder. Their results indicated that HNTs were well dispersed in polypropylene (PP) matrix and the novel vane extruder had well mixing capacity.

As to the evaluation of mixing, methods have been proposed over the past years. However, no one of them is able to quantify all aspects of mixing for every process, for example, segregation scale, distribution index and mixing efficiency are restricted to distributive mixing while mixing index is limited to dispersive mixing. So it is needed to combine these multiple methods to analyze the mixing performance comprehensively. Dhakal *et al.*[23] found that the commonly used mixing index was actually unable to predict the ranking of dispersive mixing performance because it did not reflect the magnitude of stress or the probability of particle passing the local region around the node for computing the index. Vyakaranam *et al.*[24] evaluated the air bubble dispersion by combining mixing index and shear stress, and the highest shear rate values were found in the simple shear flow region (mixing index=0.5) while the local shear rate values are much lower in the other regions (mixing index<0.4 and mixing index> 0.6). Liu *et al.*[25] comprehensively analysed residence time, segregation scale, mixing index, and instantaneous efficiency between pin unit and screw unit with or without vibration, and found that the pin unit and the vibration field could lead to alternating diffluence and rearrangement, and good flow states, respectively. Therefore, the pin unit with vibration field showed better performance of fluidity and plasticization for polymer melt particles consequently compared with the others. This comprehensive approach provided a reference for the evaluation of newly designed mixing or plasticizing devices.

More recently, we developed a novel set of torsion elements, and analyzed their heat transfer characteristics in the homogenizing section of screw using three-dimensional (3D) finite element method (FEM).[6,26] In this work, we aim to analyze and evaluate the homogenization of polymer melt by the single screw with torsion elements in homogenizing section using CFD. The case of single screw without torsion elements was also simulated for comparison.

Models and Materials

Physical Model. Here we focus on the homogenizing section of screw and the simplified geometry model of the torsion element is illustrated in Figure 1(a). It was divided into 15 parts along the circumferential direction by torsion edges, and its axial length, outer diameter and inside diameter were 10, 30 and 25.8 mm, respectively. Between every two adjacent torsion edges, there are two surfaces that are twisted by 90°. When polymer melt flows over this region, it will be tumbled under the forces from the barrel friction and the 90°-twisted surfaces. The novel screws used in the FEM simulations was called torsion screw, since it has torsion elements regularly arranged on the surface.

As shown in Figure 1(b), seven screws were considered in the simulations, among which screw A was a traditional one for comparison and screws B-G were torsion ones. The length and diameter of the screws were 180 and 30 mm, respectively. The lead of the screw element was 30 mm, and the outer and inside diameters were the same as that of torsion element. The diameter of barrel was 30.4 mm. The fluid domain was between the barrel wall and the screws. The conventional screw has screw elements along the whole length. Each of torsion screws C, E, F had four torsion elements. These elements were the same, but were located at different coordinates along the axial direction with various separations between each other. The torsion screws B and D had six and two torsion elements, respectively, all of which were located close to the outlet side by side. The torsion screw G has torsion elements along the whole length as another contrast.

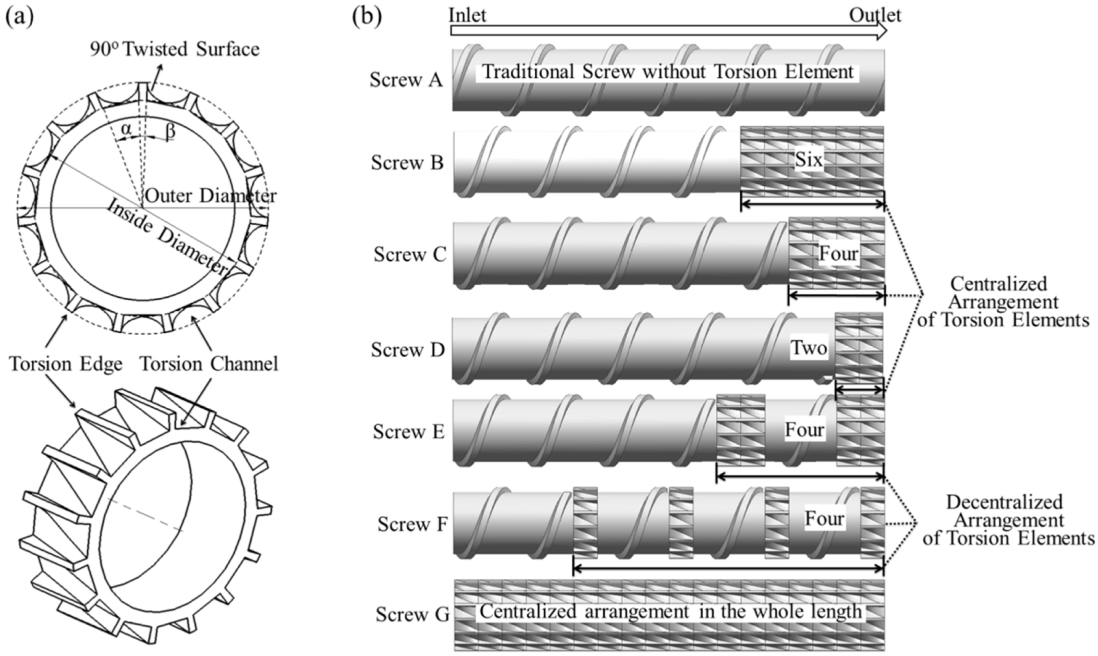

Figure 1. Geometrical configuration used in the FEM simulations for (a) the torsion element; (b) various screws with screw elements and torsion elements (designated A-G).

Mathematical Model. Polymer melt is a typical non-Newtonian fluid, being incompressible and highly viscous. It was assumed that the fluid flow was laminar and in a transient state. The fluid in the screw was a 3D non-isothermal transient flow, and non-slip conditions were applied at the wall. Since the melt was highly viscous, inertia forces were negligible compared with viscous ones. With the above assumptions, the governing equations of the flow field can be described as follows:

Continuity equation:

$$\frac{\partial u_i}{\partial x_i} = 0 \tag{1}$$

Momentum equation:

$$\rho\frac{\partial u_i}{\partial t}+\frac{\partial P}{\partial x_i} = \frac{\partial}{\partial x_j}\left(\eta\frac{\partial u_i}{\partial x_j}\right) \tag{2}$$

Energy equation:

$$\rho c_p\left(\frac{\partial T}{\partial t}+u_i\frac{\partial T}{\partial x_i}\right) = \lambda\frac{\partial^2 T}{\partial x_i^2}+\varphi \tag{3}$$

The Bird-Carreau and Arrhenius models were adopted to describe the apparent viscosity of melt, since it is dependent on both shear rate and temperature. Accordingly, the constitutive equation can be expressed as

$$\eta = \left[\eta_\infty+(\eta_0-\eta_\infty)(1+t^2\dot{\gamma}^2)^{\frac{n-1}{2}}\right]\exp\left[\alpha\left(\frac{1}{T-T_0}-\frac{1}{T_\alpha-T_0}\right)\right] \tag{4}$$

where η is the apparent viscosity, η_0 is the zero shear viscosity, η_∞ is the viscosity at an infinite shear rate, t is the natural time, $\dot{\gamma}$ is the shear rate, α is the coefficient of temperature sensibility, T_0 is the absolute zero, T_α is the reference temperature, and n is the non-Newtonian index. The physical parameters of the fluid material used in calculations are listed in Table 1, and the parameters of the screw used in calculations are listed in Table 2. ANSYS Polyflow 17.0 (ANSYS, Inc.) was used for numerical solutions, and boundary conditions are shown in Table 3.

Table 1. Physical Parameters of the Fluid Material

Density ρ	900 kg/m^3
Thermal conductivity λ	2 W/(m·K)
Specific heat capacity C_p	20 J/(kg·K)
η_0	10000 Pa·s
η_∞	100 Pa·s
n	0.75
t	0.5 s
α	2000 K^{-1}
T_α	200 °C
T_0	-273 °C

Table 2. Physical Parameters of the Screw Material

Density ρ	8030 kg/m^3
Thermal conductivity λ	16.27 W/(m·K)
Specific heat capacity C_p	502.4 J/(kg·K)

Table 3. Boundary Conditions

Location	Flow boundary conditions		Thermal boundary conditions
Inlet	Inflow	Fully developed	180 °C
		Mass flow rate 5kg/h	
Outlet	Flow outflow		Heat outflow
Barrel wall	No-slip wall		Flux density 500 W/m^2
Screw wall	Screw speeds 60 r/min		Insulated boundary /Symmetry

Methods and Grid Independence. The mixing of polymer melts was evaluated as follows:

Segregation scale, which represents the size of the regions with homogeneous concentration, was defined as[27]

$$S(t) = \int_0^{\xi} R(r,t)dr \tag{5}$$

where

$$R(r,t) = \frac{\sum_{j=1}^{M}(c_j' - \bar{c})(c_j'' - \bar{c})}{M\sigma_c^2} \tag{6}$$

$R(r, t)$ is the Eulerian coefficient of correlation between concentrations of pairs of points in the mixer separated by r, with $R(0, t)$=1 for points having the same correlation and $R(\xi, t)$=0 for those without correlation. σ_c^2 and M are sample variance and the number of pairs separated by r, respectively. The concentrations of points in the j-th pair are c_j' and c_j'', and $\bar{c}$ is the average concentration of all points. $S(t)$ is an indication of the average size of segregated regions and decreases when mixing is improved.[28]

Distribution index of particle cluster was also used to evaluate the quality of distributive mixing, and was defined as[29,30]

$$\delta(t) = \frac{1}{2}\int_0^{+\infty} \left| f(l) - f^{\mathrm{opt}}(l) \right| dl,\ \ \delta \in [0,1] \tag{7}$$

where $f(l)$ is the probability density in distance l, i.e., distance distribution, and $f^{\mathrm{opt}}(l)$ is the ideal distance distribution. The distribution index δ is the deviation of real distribution $f(l)$ from the optimal distribution $f^{\mathrm{opt}}(l)$. When the distribution is improved, the index δ decreases. This index is dimensionless, and depends not only on the initial position of the cluster, but also on the number or material points to distribute.

Mixing index was used to consider the dispersive aspects of mixing, and was defined as[31]

$$\lambda_{\mathrm{MZ}} = \frac{|D|}{|D| + |\Omega|} \tag{8}$$

where D is the rate of strain tensor and Ω is the vorticity tensor, which are the symmetric and asymmetric components of the velocity gradient tensor, respectively. The mixing index ranges in 0-1 with 0, 0.5 and 1 being pure rotation flow, pure shear flow and pure elongational flow, respectively.[28,31]

Mixing efficiency was used to consider the kinematic aspect of mixing, and it quantifies the capacity of the flow to deform matter and to generate interfaces.[32,33]

For 3D flows, an infinitesimal surface area dA with a normal direction N was defined in the initial configuration. With time, this surface deforms; at time t, this surface area is noted as da and has a new normal direction n. The degree of area stretch l is defined as the ratio of the deformed surface da at time t over the initial surface dA:

$$l = l(X,N,t) = \frac{da}{dA} \tag{9}$$

Since the fluid is incompressible, we obtained the instantaneous efficiency

$$e_1(X,N,t) = \frac{i/l}{D} \tag{10}$$

where D is the magnitude of the rate of deformation tensor, and i is the derivative of l. The time averaged efficiency was defined as

$$\langle e_1 \rangle (X,N,t) = \frac{1}{t}\int_0^{t} e_1(X,N,t')dt' \tag{11}$$

Five thousand particles were placed at the entry of the flow field. Their initial stretching orientation was set as random, and the lifetime of the particles was 300 sec.

The 3D grid system of the screw and fluid was created by the mesh superposition technique (MST) of Polyflow 17.0 (ANSYS, Inc.). The fluid domain was discretized with hexahedral elements, and all the screws were meshed with tetrahedral elements. To note that though other setting was the same for the screws A-G, they may have slightly different grid numbers because of their structural difference. To obtain more accurate results, the gap between the screw and the barrel was divided into four layers in the radial direction, and the radial size of grid was 0.05 mm, which was much smaller than other positions. Mesh adaption was adopted in order to implement mesh refinement throughout the screw domain.

Because of the similarity of the six kinds of screw system, the convergence of the MST was checked on screw A, since all screws had the same fluid domains. A mesh of 28618 tetrahedral elements was used for the screw A. Three cases of mesh size were considered for checking. The first mesh of fluid domain had 48000 elements, which were divided into 8 layers in the radial direction, 60 parts in the circumferential direction and 100 parts in the axial direction (8×60×100). In the second case, the mesh was modified into 16 layers in the radial direction with a total element number of 96000 (16×60×100). In the final case, the mesh was further changed into 80 parts in the circumferential direction, giving a total element number of 128000 (16×80×100). The magnitudes of velocity and viscosity were taken as references to check the independence of mesh, and the obtained results for the three cases are shown in Figure 2. It is indicated that the maximal differences of velocity and viscosity between the cases with 96000 and 128000 elements is less than 1% and 3%, respectively. To balance computational efficiency and precision, the mesh with 96000 elements was adopted for the computational model of the fluid domain.

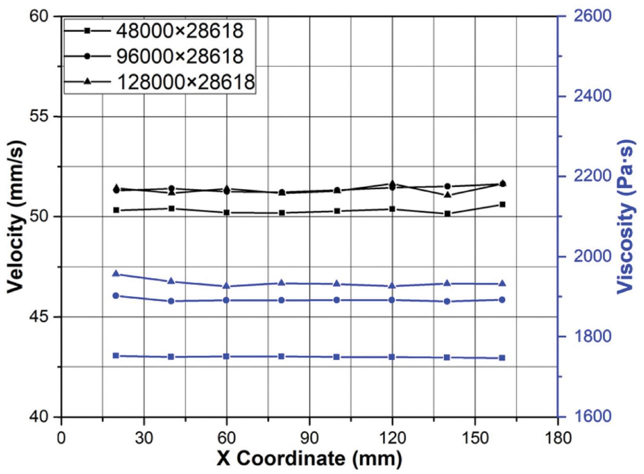

Figure 2. Velocity magnitude (left) and viscosity profile (right) of screw A using three different fluid meshes. Note that velocity magnitude and viscosity is plotted *versus* the x coordinate and there is the area-weighted average of the data points.

Results and Discussion

Mixing Ability. The segregation scales over time are given in Figure 3. It is shown that all the seven curves for the screws A-G decrease first and become stable after 12 s. From the inset of Figure 3, we can see that screw A and F have the largest and smallest stable segregation scales, respectively. These results reveal that the presence of torsion elements can reduce the separation scale and intensify mixing. More interestingly, the segregation scale curves of the screws B, C and D are greater than those of screws E and F, and that of screw E is greater than that of screw F which indicates that the segregation scale is also dependent on the arrangement of the torsion elements on the screw, and the decentralized arrangement is more effective for mixing than the centralized distribution. The stable segregation scales of the screws B, C and D are very similar, which suggests that the stable segregation scales has only weak correlations with the number of torsion elements when the elements are arranged in a centralized form. However, the segregation scales of screw G are much larger than those of other six screws, which indicated a worse mixing. Particles in one torsion channel can hardly cross the barrier into the adjacent channel, since torsion edges with centralized arrangement in screw G made up a barrier in the whole axial direction.

Figure 4 shows the distribution index over time. The results show that all seven curves of screws A-G decrease first and get stable after 25 s. The histogram of these stable values is shown in the inset of Figure 4. We can see that screw F has the small-

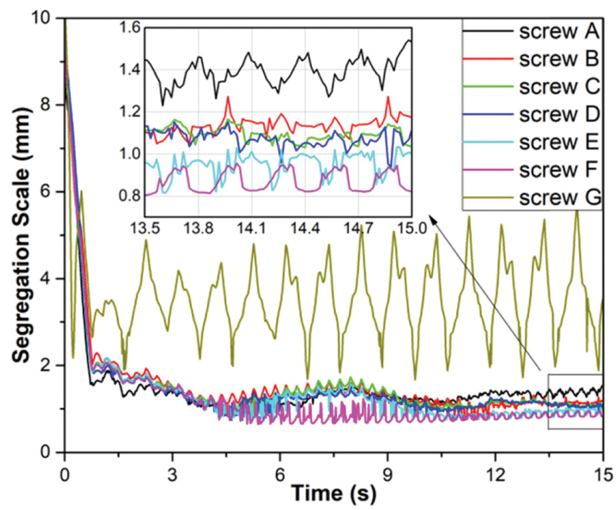

Figure 3. Evolution of segregation scale over time. The inset is the scale-up view of the marked region by the rectangle.

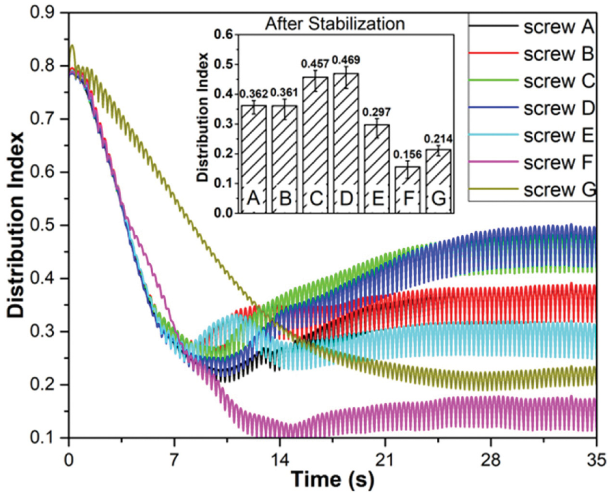

Figure 4. Evolution of distribution index over time for non-cohesive clusters. Material points were initially located at the inlet of the flow region uniformly.

est distribution index. The value of screw B is greater than that of screw E, and screw E is greater than that of screw F. These results also indicate that the decentralized arrangement is more effective for mixing than the centralized distribution from the term of distribution index. For screws C, E and F, which have the same number of torsion elements, we found that the distribution index decreases when the torsion elements are distributed in a increasingly decentralized form. It should be noted that the distribution index of screw A is almost equal to that of screw B, and is smaller than that of screws C or D. These results indicate that the effect of torsion elements with centralized arrangement on distribution index is weak in the cases with torsion element less than six. This is because the torsion edge would shackle particles in the same position of torsion channels when the torsion elements have a centralized distribution. The distribution index of screw G are second smallest among all those of seven screws. However, too many torsion elements may increase the undesired resistance and energy consumption, therefore the optimized choice is the decentralized distribution of appropriate number of torsion elements along the screw.

Mixing Efficiency. The mean instantaneous and time averaged mixing efficiencies are shown in Figure 5 and Figure 6, respectively. The two figures show that screws B-F with torsion elements are significantly more efficient for mixing than screw A. In Figure 5, after several revolutions, the curves of screws B-F show a sudden rise, and maintain on a relatively larger level compared with that of screw A. The rise in the curves for the screws with torsion elements appears in the order of F, E, B, C, and D, which indicates that the decentralized arrangement of torsion elements is more efficient for mixing than the centralized distribution.

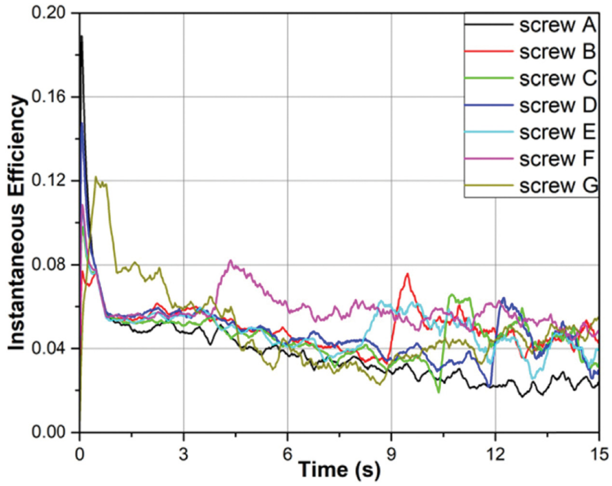

Figure 5. Mean instantaneous mixing efficiency over time.

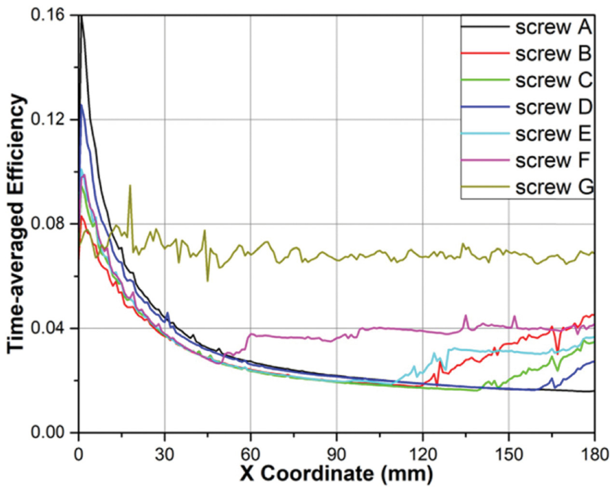

Figure 6. Time averaged mixing efficiency *versus* the X coordinate in 15 s.

Figure 6 gives the evolution of the time averaged mixing efficiency along the axis for the seven considered screws. As the axial coordinate increases, all the curves of screws decrease in general except that of screw G. Specifically, the time averaged mixing efficiency for screws B-F shows a rise at coordinates of 120, 140, 160, 110, 50 mm, respectively. These positions are just where the fronts of the first torsional elements were located. Out of all the screws except screw G, screw F has the maximal time averaged mixing efficiency in total. These results indicate that the torsion elements with a decentralized arrangement can improve the time averaged mixing efficiency in total.

Plasticizing Quality. To evaluate the plasticizing quality, the distributions of temperature and viscosity in the cross section of outlet were calculated and are shown in Figure 7. Figure 7(a) and Figure 7(b) are the temperature distributions at position of outlet for the screw A and Screw F, respectively. Figure 7(a) reveals that the temperature distribution in the cross section is non-uniform with a range of 297.2-299.6 ºC. The temperature is high near the screw flight and is low far away from the screw flight. However, Figure 7(b) reveals that the temperature distribution in the cross section is relatively uniform with a range of 299.0-299.4 ºC. Figure 7(c) and Figure 7(d) are the viscosity distributions at position of outlet for the screw A and Screw F, respectively. Figure 7(c) reveals that the viscosity is inhomogeneous in the cross section with a viscosity of 2600 Pa·s in most regions and lower than 700 Pa·s in part of the left regions. These results may be because of the high shear stress and high temperature near the screw flight. However, Figure 7(d) shows that the viscosity distribution in the cross section for Screw F are mostly in the range of 2000-2200 Pa·s. Due to the good mixing capability of torsion screw F, both distributions of temperature and viscosity are more uniform at the position of outlet than those of screw A without torsion elements. By the way, other five torsion screws B-E and G also have better uniformity of temperature and viscosity

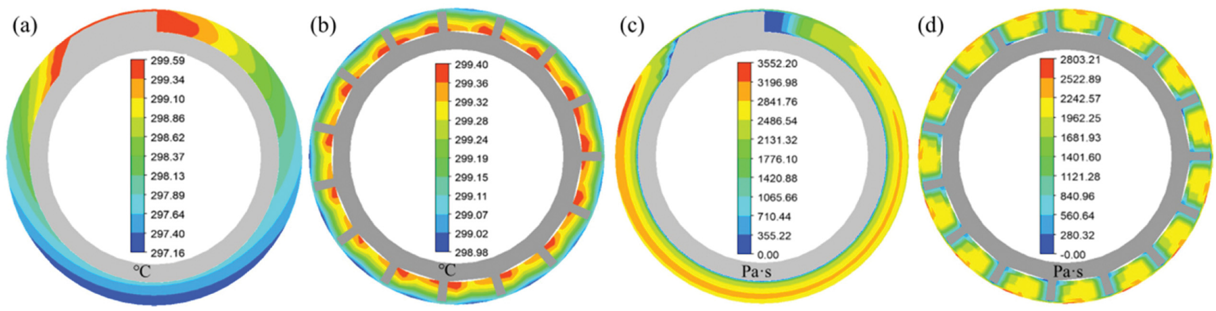

Figure 7. Distributions of temperature and viscosity at position of outlet for screw A (a and c) and screw F (b and d), respectively. The screw is shown in gray.

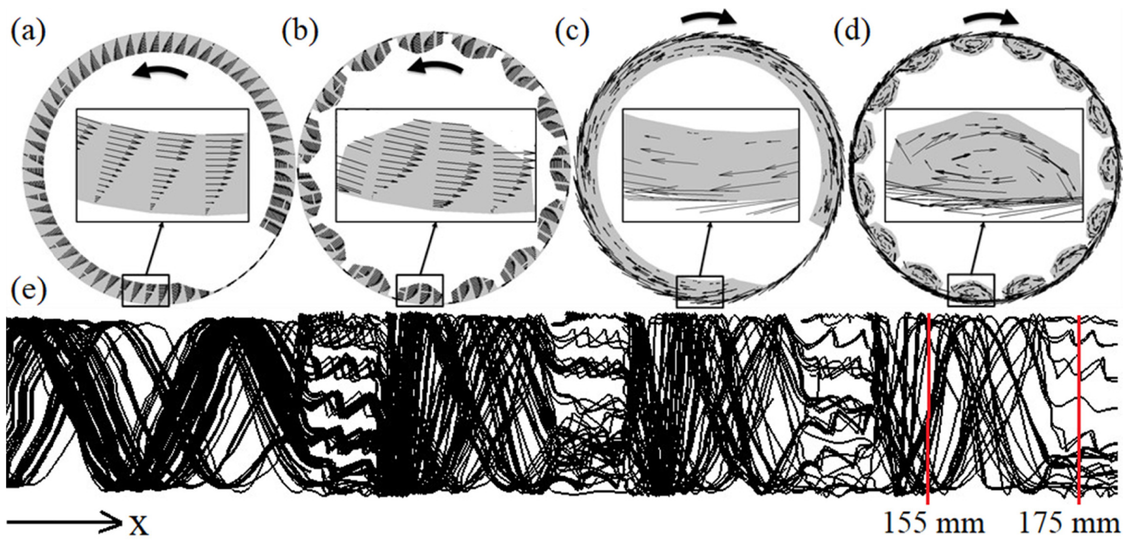

Figure 8. Velocity vectors in the axial cross section for the screw element (a and c) and torsion element (b and d) and velocity streamline of screw F (e). The velocity vector is shown by the direction of arrow and the magnitude of velocity is shown by the length of arrow. Screw F at X coordinates of (a) 155 mm and (b) 175 mm in the inertial reference frame where the barrel is fixed and the screw rotates counterclockwise. The marked regions by the rectangules are scaled up for clear view. Screw F at X coordinates of (c) 155 mm and (d) 175 mm in the rotating reference frame where the barrel is rotating clockwise and the screw is fixed. The X coordinates of 155 mm and 175 mm are where the screw and torsion elements located, respectively. Velocity streamline of screw F is in the rotating reference frame.

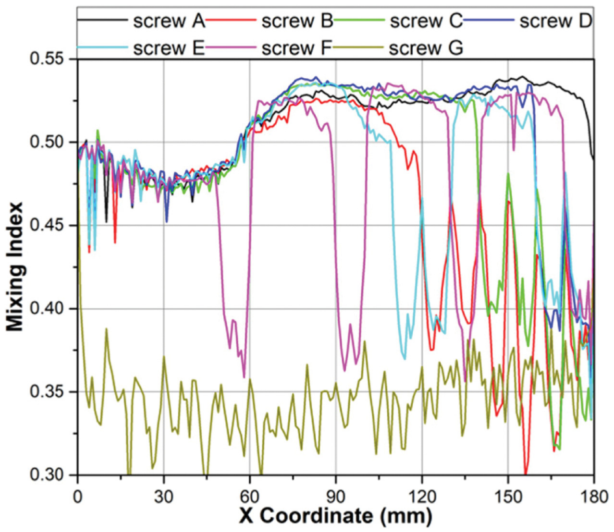

Figure 9. Mixing index *versus* X coordinate for screws A-G. Values of 0, 0.5 and 1 represent pure rotation, pure shear and pure elongation, respectively.

than that of conventional screw A in the cross section of outlet.

Velocity Field and Flow Characteristics. In order to get insights into the effects of torsion elements on the mixing behavior of polymer melt in the screw system, the velocity field and characteristics of the flow were investigated. The velocity vectors in the axial cross section for the screw element and torsion element in both the rotating and inertial reference frames are shown in Figure 8(a)-(d). With the velocity profiles in the channel of screw system, it is possible to analyze the mixing capability of each screw. Even though the fluid has the similar velocity vectors in the regions of screw and torsion elements in the inertial reference frame in Figure 8(a) and 8(b), local rotational flows appear in the region of torsion element revealed by the velocity vectors in the rotating reference frame in Figure 8(d), which is not observed in the region of screw element in Figure 8(c). The local rotational flow would enhance mass transfer in the radial direction, which can accelerate mixing. Velocity streamline of screw F in the rotating reference frame is shown in Figure 8(e). It further confirms the existence of spiral flow near the torsion element.

Figure 9 gives the axial evolution of mixing index for the seven considered screws. It can be found that the seven curves are all below 0.55, and are closer to 0.5 than to 1, implying that the particles are mostly in a shear flow. It is interesting that the mixing index in the regions of torsion elements is much smaller than that of screw elements for all the seven consider cases. In the regions of torsion elements, the mixing index is in the range of 0.3-0.4, especially for screw G, which also suggests that the particles are partly in a rotational flow.

Combined with the velocity vectors and streamline in Figure 8(d) and 8(e), the results indicated that a rotational flow occurs at the position of torsion element owing to the unique torsion structure of element. This radial mass displacement is beneficial to mixing, convection heat transfer, and plasticizing uniformity.

Conclusions

In this work, a series of screws with torsion elements and screw elements were investigated by numerical simulations to examine their mixing and plasticizing ability. The mixing was evaluated from separation scale, distribution index, and mixing efficiency. The obtained results suggest that the screws with torsion elements arranged in a decentralized form have smaller segregation scale, distribution index and higher mixing efficiency, compared with the conventional screw. The decentralized arrangement is more effective for mixing than the centralized distribution. The mixing efficiency is strongly related to the starting set position of the torsion element.

The rotational flow induced by the torsion elements can significantly enhance the mass transfer process and improve mixing and plasticizing. Compared with those in conventional screw, the distributions of temperature and viscosity are more uniform at the outlet of torsion screws, which also made the torsion element generally more effective and efficient for mixing and plasticizing.

The separation scale and the distribution index are not exactly consistent in the evaluation of mixing performance, which has also been reported in previous work.[34] This confirms that we have to combine multiple methods and factors to comprehensively evaluate the mixing capability of screw.

Acknowledgement: This work was supported by the National Natural Science Foundation of China (No. 51576012), the National Key R&D Program of China (No. 2016YFB0302000) and the Fundamental Research Funds for the Central Universities (No. BHYC1704A).

References

1. H. Potente and W. H. Tobben, *Macromol. Mater. Eng.*, **287**, 808 (2002).
2. J. W. Sikora and B. Samujlo, *Polym. Eng. Sci.*, **54**, 2037 (2014).

3. J. N. Chen, P. Dai, H. Yao, and T. Chan, *J. Polym. Eng.*, **31**, 53 (2011).
4. C. Rauwendaal, *Plast. Add. Compound.*, **10**, 32 (2008).
5. K. Y. Lee, *Polym. Korea*, **22**, 174 (1998).
6. R. Jian, W. Yang, L. Cheng, and P. Xie, *Inter. J. Heat Mass Transfer*, **115**, 946 (2017).
7. T. Taguchi and H. Saito, *J. Appl. Polym. Sci.*, **133**, 7 (2016).
8. M. S. Kang, B. Y. Kang, H. S. Sim, J. M. Son, K. H. Lee, and M. Park, *Polym. Korea*, **35**, 99 (2011).
9. W. R. Hwang, K. W. Kang, and T. H. Kwon, *AICHE J*., **50**, 1372 (2004).
10. W. G. Yao, S. Tanifuji, K. Takahashi, and K. Koyama, *Polym. Eng. Sci.*, **41**, 908(2001).
11. X. Li, J. Peng, and J. Chen, *China Plastics*, **24**, 109 (2010).
12. G. Zitzenbacher, R. Karlbauer, and H. Thiel, *Int. Polym. Process.*, **22**, 73 (2007).
13. P. Kubik, J. Vlcek, C. Tzoganakis, and L. Miller, *Polym. Eng. Sci.*, **52**, 1232 (2012).
14. W. Hu, X. Luo, and Z. Yan, *Polym. Korea*, **41**, 944 (2017).
15. Y. H. Feng, J. P. Qu, H. Z. He, B. Liu, X. W. Cao, and S. P. Wen, *J. Appl. Polym. Sci.*, **108**, 3917 (2008).
16. M. Bouquey, C. Loux, R. Muller, and G. Bouchet, *J. Appl. Polym. Sci.*, **119**, 482 (2011).
17. J. P. Qu, Z. T. Yang, X. C. Yin, H. Z. He, and Y. H. Feng, *Polym.-Plast. Technol. Eng.*, **48**, 1269 (2009).
18. J. P. Qu, X. Q. Zhao, and J. B. Li, *Adv. Mater. Res.*, **472**, 1941 (2012).
19. X. C. Yin, S. Li, G. J. He, G. Z. Zhang, and J. P. Qu, *Adv. Polym. Technol.*, **35**, 215 (2016).
20. J. S. Wen, S. K. Lei, Y. H. Liang, X. F. Peng, and J. P. Qu, *J. Macromol. Sci. Part B-Phys.*, **53**, 358 (2014).
21. J. S. Wen, Y. H. Liang, and Z. M. Chen, *Adv. Mater. Res.*, **421**, 415 (2012).
22. X. Yin, S. Li, L. Wang, G. He, and Z. Yang, *Polym. Korea*, **41**, 163 (2017).
23. P. Dhakal, S. R. Das, H. Poudyal, and A. J. Chandy, *J. Appl. Polym. Sci.*, **134**, 9 (2017).
24. K. V. Vyakaranam and J. L. Kokini, *Chem. Eng. Sci.*, **84**, 303 (2012).
25. T. L. Liu and Y. X. Du, *Polym.-Plast. Technol. Eng.*, **50**, 1231 (2011).
26. R. Jian, P. Xie, and W. Yang, *J. Eng. Thermophys.*, **38**, 281 (2017).
27. P. V. Danckwerts, *Appl. Sci. Res. A*, **3**, 279 (1952).
28. J. Wei, D. Chen, D. Zhou, A. Zhang, and Y. Yang, *Polym. Korea*, **39**, 441 (2015).
29. T. H. Wong and I. Manas-Zloczower, *Int. Polym. Process.*, **9**, 3 (1994).
30. H. H. Yang and I. Manas-Zloczower, *Int. Polym. Process.*, **9**, 291 (1994).
31. J. J. Cheng and I. Manas-Zloczower, *Int. Polym. Process*., **5**, 178 (1990).
32. J. M. Ottino, W. E. Ranz, and C. W. Macosko, *AICHE J.*, **27**, 565 (1981).
33. J. M. Ottino, *The Kinematics of Mixing: Stretching, Chaos, and Transport*, Cambridge University Press, Cambridge, UK, 1989.
34. R. K. Connelly and J. L. Kokini, *J. Food Eng.*, **79**, 956 (2007).

Nomenclature

ρ = density, kg/m^3
C_p = specific heat capacity, J/(kg·K)
λ = thermal conductivity, W/(m·K)
T = temperature, K
x_i, x_j = cartesian coordinates, m
u_i = velocity vector, m/s
μ = viscosity, Pa·s
P = pressure, Pa
η = apparent viscosity, Pa·s
η_0 = zero shear viscosity, Pa·s
η_∞ = viscosity at an infinite shear rate, Pa·s
t = natural time, s
α = temperature sensibility coefficient, K^{-1}
n = non-Newtonian index
T_α = reference temperature, °C
T_0 = absolute zero, °C